High Dynamic Range Wide Bandwidth Imaging

W. D. Cotton March 15, 2010

***Abstract*—This memo describes a technique of wide-band interferometric deconvolution adapted for high dynamic range applications. The general method is to divide the bandpass into relatively narrow band segments, image each with approximately constant resolution, do a coupled CLEAN deconvolution and finally fit a spectral form to each pixel. The deconvolution features CLEAN components with a coarse, tabulated spectrum which can be used for self calibration as is always needed for high dynamic range imaging. The output of this process is a set of images with the flux density, spectral index and one or more curvature terms and images in each of the coarse channels. Frequency dependent primary beam gain can be corrected in the imaging and spectrum fitting. A dynamic range in excess of 10^5 was achieved for a challenging simulated data set. A working implementation is available as an Obit task.**

***Index Terms*—Wide-band Imaging, Interferometry**

I. Introduction

ONE of the principle ways in which radio interferometer arrays currently under construction or in planning increase their sensitivities over current arrays is by a large increase in the bandwidth being sampled. This presents challenges to imaging the data from the new arrays as the large bandwidths violate one of the traditional implicit assumptions used in imaging, that the sky looks the same at all frequencies in the observed bandpass. This assumption can be relaxed somewhat by assuming that all the emission in the image has the same spectral shape but with a sufficiently wide bandpass and a range of spectral shapes in the primary antenna pattern, this assumption breaks down.

To reach the sensitivity which the new instruments are in theory capable, all of the sky in which there are detectable sources must be imaged in order to remove the side–lobes of these sources. At lower frequencies this essentially means that the entire primary beam must be imaged along with selected areas in the side-lobes. Thus, especially at lower frequencies, a wide-band imaging problem is also a wide-field imaging problem. This increases the potential for a range of spectral shapes in the image. High dynamic range imaging requires some variation on the source estimation and subtraction from the visibility data (e.g. "Cotton–Schwab" CLEAN of [1], [2]) which is needed to suppress the aliasing resulting from the use of FFTs. A further requirement is that the imaging/deconvolution produce a sky model that can be used for self calibration.

II. Previous Work

Sault and Wieringa [3] developed a technique for deconvolving wide-band radio synthesis data using a set of convolutions of residual images and beams. This technique was examined in [4] which concluded that it was not suitable for high dynamic range imaging of extended sources. The fundamental problem appears to be an ambiguity between source spectrum and frequency variable surface brightness sensitivity. This problem is examined in more detail.

A previous attempt at high dynamic range wide-band imaging using multiple sub–band images is described in [5]. Several of these techniques resulted in good dynamic range on simulated datasets but had operational difficulties, in particular, the inability to use the resultant image as a self–calibration model. In this memo, these techniques are further explored and expanded into an operationally viable technique. This development used the Obit ([6], http://www.cv.nrao.edu/∼bcotton/Obit.html) package.

III. Multiple Sub–band Imaging

Ignoring the spectral variation of the sky brightness in deriving images from data with wide bandpasses will result in image artifacts arising from this variation, as is demonstrated below. Images made with sufficiently narrow bandpasses will not suffer from these artifacts. Therefore, a set of narrow band images will represent the sky emission in a wide-band dataset without these artifacts but suffers from the limited sensitivity in each narrow band image. The following sections explore several possibilities for deriving wide-band images using cubes of images derived from sub bands of the total observed spectrum. These are extensions of the techniques in [5].

A. Test Data

Each of the imaging possibilities were tested using one of the simulated test datasets from [5]. This test dataset was derived from a 15×390 kHz channel VLA dataset at 1.4 GHz with 1 "IF" involving multiple snapshots. This was expanded to 10 IFs spaced at 100 MHz intervals which (sparsely) covers the range 1.4 to 2.3 GHz. The data values were replaced by the Fourier transform of the model whose parameters are given in Table I. The model was originally calculated at a reference frequency of 1.417 GHz but is given in Table I at 1.867, the reference frequency used for imaging. A small amount of zero mean Gaussian pseudo noise was added.

The image of this data as derived from a traditional method ignoring spectral properties as well as a spectrally sensitive rendition from [5] are shown in Figure 1. The dynamic range[1] obtained by ignoring the spectral variation is about a factor of 75 worse than a spectrally sensitive rendition which was itself limited by systematics.

National Radio Astronomy Observatory, 520 Edgemont Rd., Charlottesville, VA, 22903 USA email: bcotton@nrao.edu
Manuscript received ; revised

[1]Dynamic range in this memo is defined as the ratio of the image peak to off source RMS

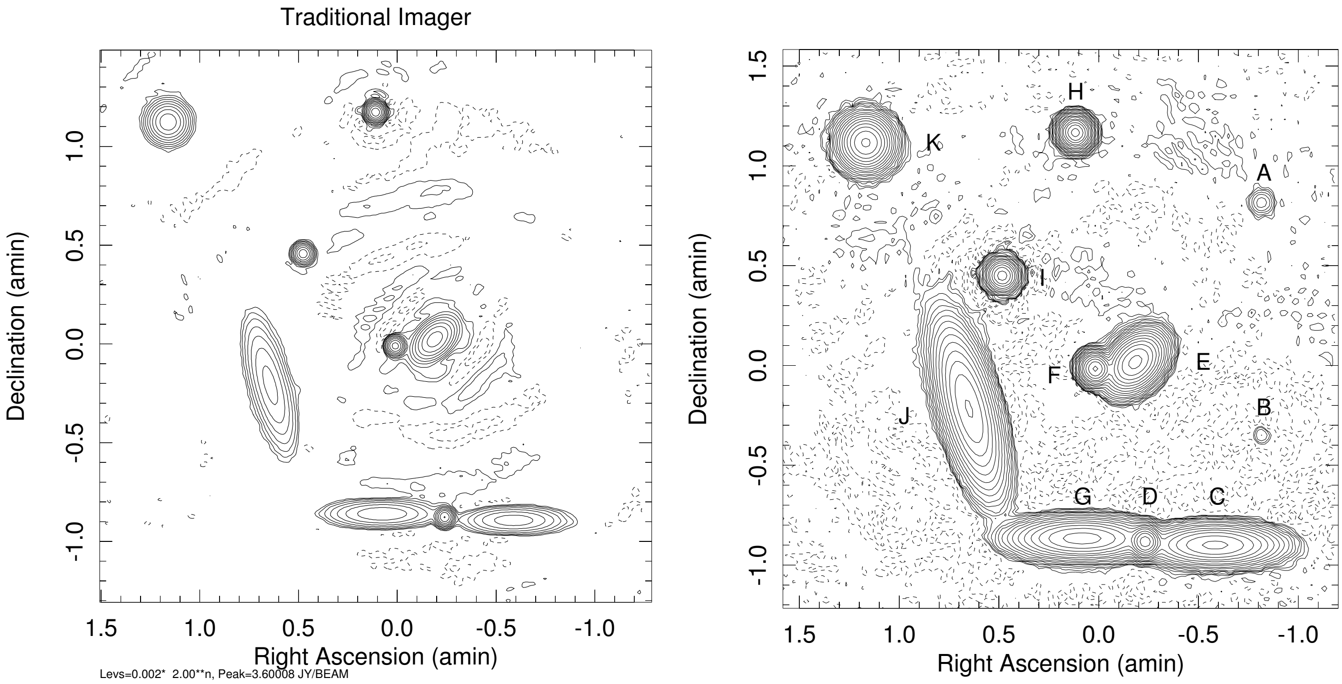

Fig. 1. **Left:** Multiple component model given in Table I with added noise. Traditional imaging ignoring spectral variations. The image RMS is 0.94 mJy/bm and dynamic range is 3.8×10^3. Contour levels are powers of 2 from 2 mJy/bm, the peak in the image is 3.6 Jy/beam. Negative contours are dashed.
Right: Spectral fitting s_{ν_0} results from [5]. The image RMS is 0.014 mJy/bm and the dynamic range is 2.8×10^5 Contouring uses levels spaced by powers of 2.0 from 2.0×10^{-2} mJy/beam, one hundred times lower than on **Left**. Resolution is that of the lowest frequency. Components are labeled as given in Table I.

TABLE I
"Multi" Model Parameters @ 1.867 GHz

	X ”	Y ”	S Jy	α	β	Maj ”	min ”	PA °
A	-50.0	50.0	0.001	0.0	0.0	0.0	0.0	
B	-50.0	-20.0	0.0002	0.0	0.0	0.0	0.0	
C	-36.0	-53.0	1.63	-0.76	-0.01	15.0	3.0	90.0
D	-15.0	-52.0	1.07	0.25	0.0	0.0	0.0	
E	-12.0	2.0	3.53	-1.27	-0.033	7.0	4.0	135.0
F	0.0	0.0	1.5	0.0	0.0	0.0	0.0	
G	4.0	-51.0	2.08	-0.68	-0.05	16.0	3.0	90.0
H	6.0	71.0	3.71	0.17	-0.15	0.0	0.0	
I	28.0	28.0	1.0	0.0	0.0	1.0	1.0	
J	38.0	-12.0	2.57	-0.56	-0.025	20.0	5.0	15.0
K	69.0	68.0	3.92	-0.11	-0.10	5.0	5.0	

B. Spectral Representation

Astrophysical sources of broadband emission generally emit by either thermal or synchrotron mechanisms. In either case, the spectral shape over large areas of the radio spectrum are close to a power law. This suggests the form of the spectrum to be adopted. The technique presented here uses the following adaptation of the traditional representation of a continuum source spectrum:

$$s_\nu = s_{\nu_0}\ e^{\alpha\ log(\nu/\nu_0)\ +\ \beta\ log(\nu/\nu_0)^2\ +...}$$

where s is the spectral flux density, ν is frequency, ν_0 a reference frequency and α, β, ... are the "spectral index" and one or more curvature terms. As many terms can be used in the exponent as are needed to accurately represent the observed emission. This is the same as the traditional scalar pixel representation with the addition of the exponential term to give the spectral shape.

IV. Spectral Imaging Revisited

The "Spectral Imaging" imaging technique of [5] had disappointing results but had the operational advantage that the deconvolution produced CLEAN components with parameterized spectra. This technique as practiced in [5] consisted of estimating the spectral parameters in each pixel prior to the inner Clark CLEAN loop. Storing the spectral information on the CLEAN components made use of modifications described in [5] and is generally supported in the Obit SkyModel classes.

A variant of this was tried, in which the fitting and deconvolution was fully done in the inner loop. The first test was using the coarse spectral image planes at their natural, frequency dependent resolution. The image from this test is shown in Figure 2 **left** and has a dynamic range of 3.7×10^3; i.e. no improvement over ignoring the spectral variations. An examination of the residual coarse spectral images revealed the cause of the very poor behavior. Point sources were well modeled but the fitted spectra in extended sources poorly represented the sources, being much too steep. At the lower frequencies, the center portion of images of extended components had deep holes while at high frequencies they contained high peaks. The channel residual images around the strongest extended source is shown in Figure 3.

Following the technique of [5] a second test was performed in which the spectral planes were tapered to obtain approximately a constant resolution.

The frequency dependent taper was derived from the desired CLEAN restoring beam (CB_*, size in asec) by first computing a "correction" Gaussian, the convolution of which with the dirty beam at each frequency would give the desired size beam. This was computed as follows for each frequency $Freq$:

$$target_{major} = \left(\frac{refFreq}{Freq}\right) \times CB_{major}$$

$$target_{major} = \left(\frac{refFreq}{Freq}\right) \times CB_{minor}$$

where $refFreq$ is the imaging reference frequency. The convolving Gaussian for this frequency was then

$$corr_{major} = \sqrt{CB^2_{major} - target^2_{major}}$$

$$corr_{major} = \sqrt{CB^2_{minor} - target^2_{minor}}$$

$$corr_{posAngle} = CB_{posAngle}$$

. The parameters of the elliptical Gaussian taper used for this frequency were:

$$taper_{major} = (fudge/((corr_{major}/2.35)/206265.0))/\pi$$

$$taper_{minor} = (fudge/((corr_{minor}/2.35)/206265.0))/\pi$$

$$taper_{posAngle} = (corr_{posAng}),$$

where image plane Gaussian sizes are in arcseconds and uv plane sizes in wavelengths. The CLEAN restoring beam can be determined by making the beam for the lowest frequency data and fitting a Gaussian. The fudge factor ($fudge$) is to correct for the sparseness of the UV coverage, in the following tests, a value of 0.80 was used. The fudge factor depends of the distribution and weighting of the data and needs to be determined empirically.

The result of this test is shown in Figure 2 **right** and obtained a dynamic range of 3.3×10^4. This result is an order of magnitude improvement on the previous test but nearly an order of magnitude worse that the best result from [5]. The improved behavior is due to the better representation of the channel images; the residuals of which are shown in Figure 4 with the same contouring as Figure 3. Tapering the data to obtain a relatively constant resolution with frequency appears vital.

V. Spectral Fitting Revisited

Following the development in [5], a test was made of "Spectral Fitting". This is similar to Spectral Imaging in that the imaging produces a coarse resolution spectral cube but the planes of these cubes are deconvolved using CLEAN before fitting the spectra. The major difference in the current development and that of [5] is that the deconvolution among planes is coupled. A combined image (linear average of the coarse frequency channels) is used to drive the CLEAN process, in particular, to pick the location of CLEAN components. The CLEANing then uses the spectrum from the coarse set of channel images to determine the flux density to be removed from that pixel. This produces a separate but coupled deconvolution of each of the channel images. After the deconvolution is complete and each of the planes has the CLEAN components restored, a spectrum is fitted on a pixel–by–pixel basis and the resultant image is composed of image planes for flux at the reference frequency, spectral index, and any curvature planes. In the implementation described here, the restored, coarse image planes follow the spectral parameter planes in the resultant image cube.

A. Clean Component Representation

The use of individual channel flux densities requires an extension of the concept of CLEAN components. The distinction is made between CLEAN components with "parameterized" spectra ($\alpha,\ \beta,\ \ldots$) and tabulated spectra (flux densities at a list of frequencies). The latter is practical as only a dozen or so frequency channels are needed to represent the spectrum. A CLEAN component table containing tabulated spectra can be used as a frequency sensitive sky model.

B. Fitting Spectra

Fitting the spectra to the pixel flux densities must take into account the varying sensitivity and antenna gain as a function of frequency. The RMS "noise" is determined in each plane and adjusted by the frequency dependent antenna gain as is the flux density. The fitting is by weighted least squares. The lowest order fit giving an adequate χ^2 is adopted to avoid erratic fitting results in low signal-to-noise pixels.

C. Epicycles and Deferents

In practice, there are conditions that arise in the above procedure that can cause problems. Corrections for these potential difficulties introduce other problems whose fixes cause yet other problems, etc. The following corrections are currently thought to adequately deal with these.

1) Epicycle A: Picking components on the basis of the summed flux can ignore pixels with channels with significant flux when the flux density in all channels sums to zero.
Solution A: Clip residuals at 5 sigma from average and add 10% of the most extreme channel flux to the sum of the channels, This forces CLEAN to pay attention to these pixels and clean the channels differently.

2) Epicycle B: **Solution A** introduces threshold effects causing "out of band noise" which can drive into oscillations, digging and filling holes.
Solution B: Convolve the extrema image with the dirty beam before adding – this causes the combined image to be a convolution which makes the CLEAN more robust.

3) Deferent C: **Solution B** broadens the response to the extrema causing "significant" pixels in which all channel flux densities are themselves insignificant. "CLEANing" them has no effect on the image. When these dominate the CLEAN cycle, CLEAN is trapped in a loop with negligible effect of

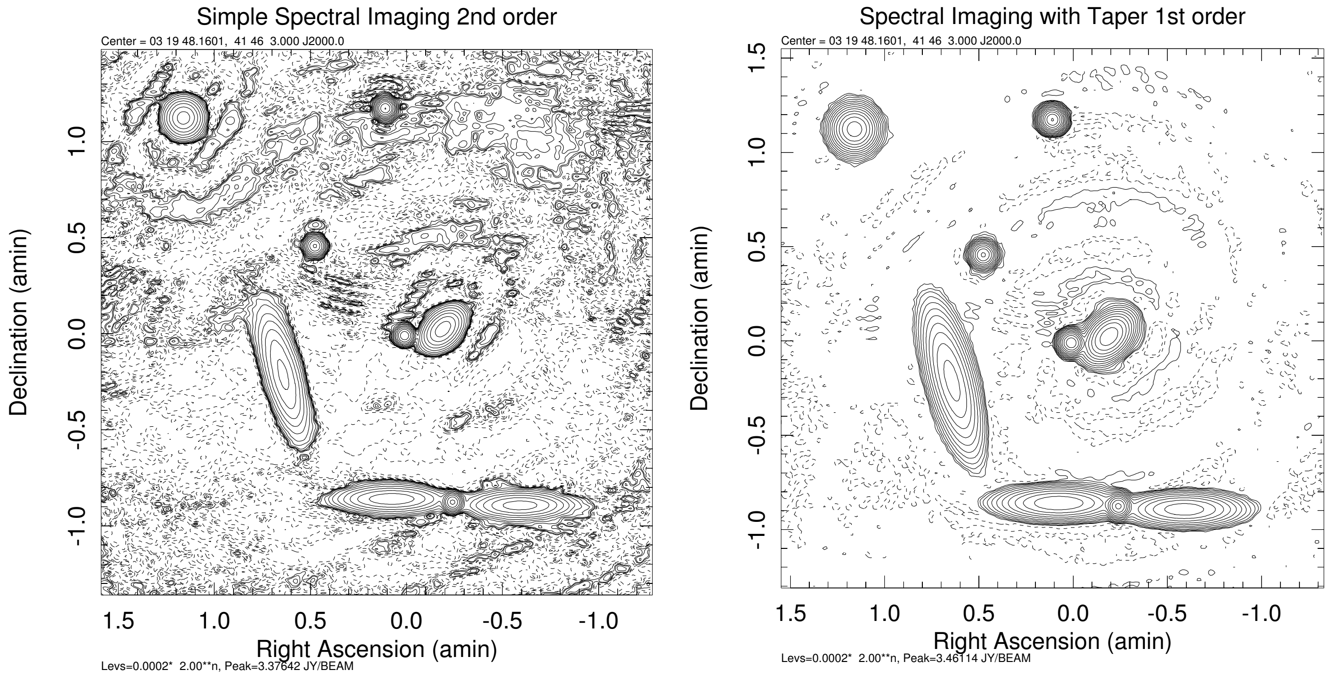

Fig. 2. **Left:** Image of test data derived from simple application of Spectral imaging. The image RMS is 0.9 mJy/bm and dynamic range is 3.7×10^3. Cell spacing is 0.6”. Contour levels are powers of 2 from 0.2 mJy/bm, the peak in the image is 3.38 Jy/beam. Negative contours are dashed.
Right: Image of test data derived from spectral imaging tapering the channels to (approximately) the same resolution. The image RMS is 0.1 mJy/bm and dynamic range is 3.3×10^4. Cell spacing is 0.6”. Contour levels are powers of 2 from 0.2 mJy/bm, the peak in the image is 3.46 Jy/beam.

the residual image.
Solution C: When picking components for the inner clean, ignore pixels for which the most extreme channel residual value is less that the combined flux density.

D. Test Results

When the spectral fitting+correction procedure was applied to the test data set, the images shown in Figure 5 was obtained. The dynamic range obtained was 1.2×10^5. The residual image is still dominated by systematic effects and has about a factor of 2 lower dynamic range than derived in [5] with completely independent CLEANs in the different channels. Gaussians were fitted to the image in Figure 5 and spectral index and curvature terms (when fitted) are interpolated at the peak and given in Table II; the agreement with the input model in Table I is excellent.

VI. Self–calibration

The test data used in the tests described above had no systematic calibration errors but can still be used to explore the effects of the interaction of the wideband imaging process with self–calibration. Self–calibration was applied using the image resulting from the Spectral Fitting and fitting for a single phase per antenna per solution interval using Obit task Calib. When the “calibrated” data was reimaged, the resultant dynamic range was very nearly that of the pre-calibration result.

In real wideband data, a single phase per antenna is insufficient to describe the atmospheric effects. Over wide bandwidths, the group delay from the neutral atmosphere and, at lower frequencies ($<\sim$ 10 GHz), a dispersive term for the ionosphere will also be needed.

TABLE II
Fitted Parameters @ 1.867 GHz (Spectral Fitting)

	X ”	Y ”	S Jy	α	β	Maj ”	min ”	PA ○
A	-50.0	50.0	0.00098			0.0	0.0	
B	-49.9	-19.9	0.000015			0.0	0.0	
C	-36.0	-53.0	1.62	-0.76	0.009	15.4	4.8	90.0
D	-15.0	-52.0	1.07	0.24	0.005	0.0	0.0	
E	-12.0	2.0	3.53	-1.27	-0.019	7.0	4.0	135.0
F	0.0	0.0	1.50	0.00	-0.004	0.0	0.0	
G	4.0	-51.0	2.01	-0.68	-0.019	16.4	4.8	90.0
H	6.0	71.0	3.71	0.17	-0.15	0.0	0.0	
I	28.0	28.0	1.00	-0.01	0.013	1.0	1.0	
J	38.0	-12.0	2.57	-0.56	-0.017	20.0	5.0	15.0
K	69.0	68.0	3.92	-0.11	-0.10	5.0	5.0	

VII. Obit Implementation

In Obit the Spectral Fitting technique was implemented in the ObitDConCleanVis class using a number of derived subclasses. The derived specialized classes are described in the following:

- **ObitDConCleanVisMF**
  Derived from ObitDConCleanVis and does the specialized operations:
  - Performs “middle” CLEAN loop for autoWindow imaging in which the tabulated spectra on the CLEAN components are subtracted from the residual

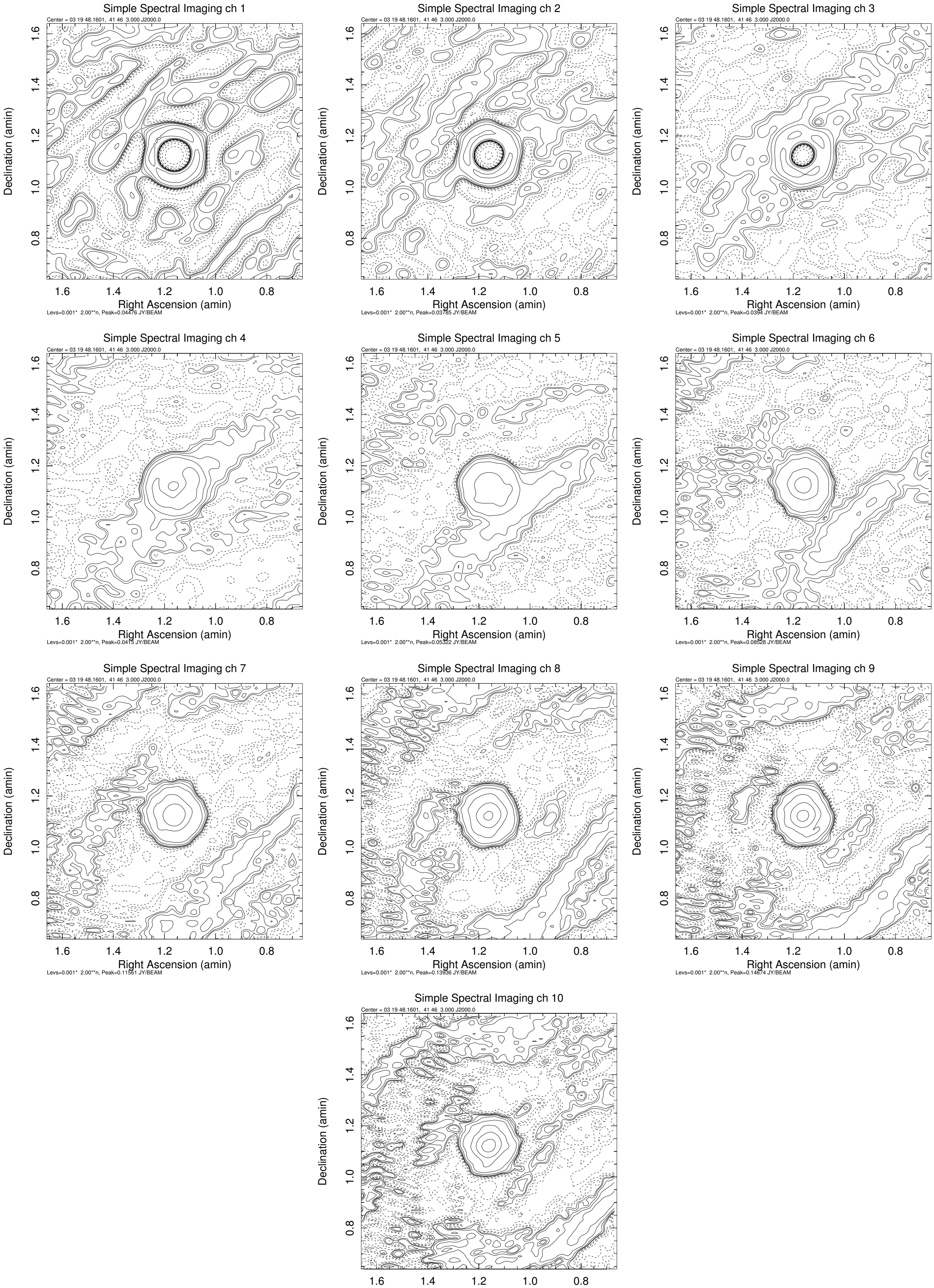

Fig. 3. Region around north–east most extended source showing spectral channel residual images after making the image in Figure 2 **left** . Contours are powers of 2.0 times 1 mJy/bm, negative contours are dashed.

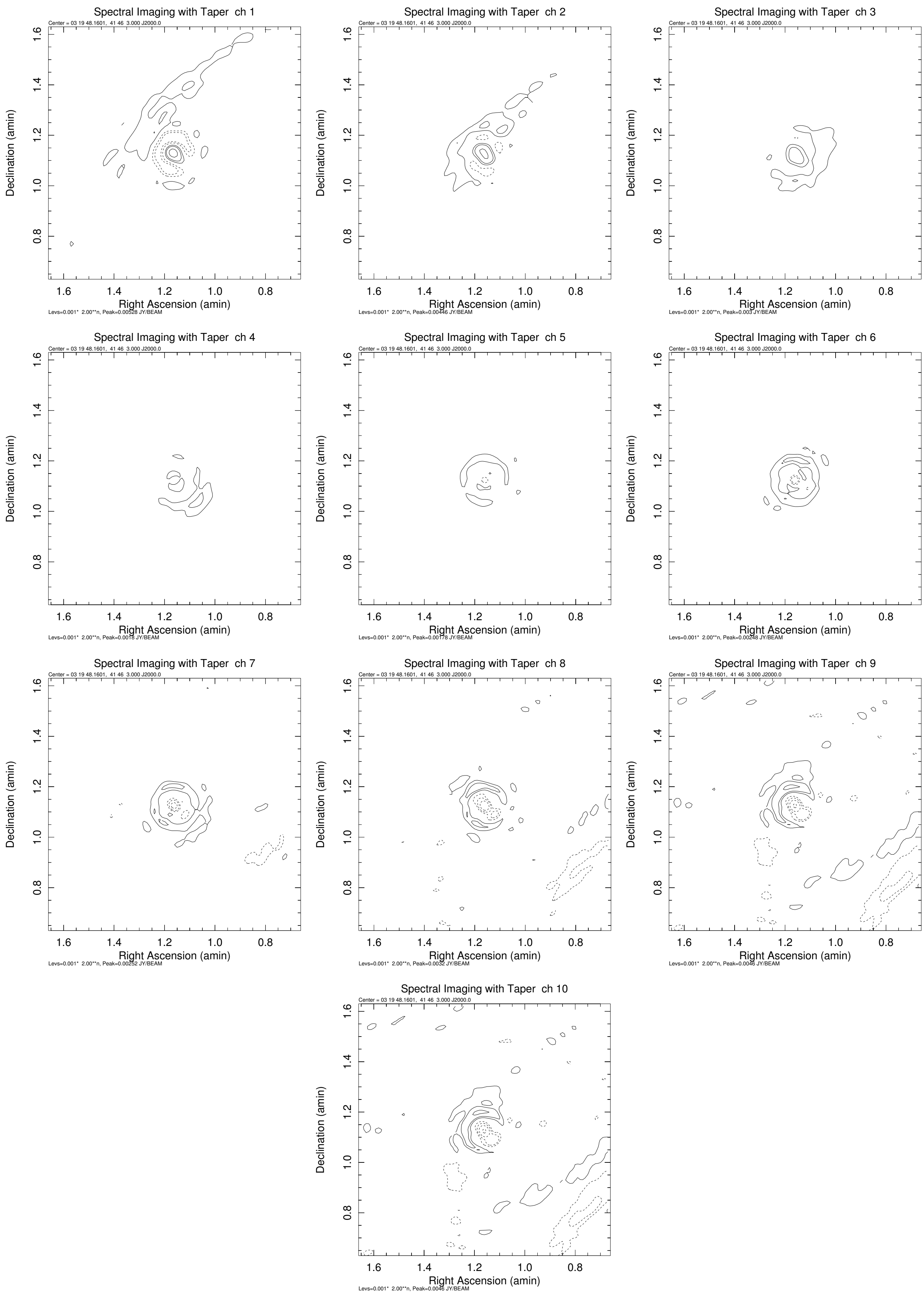

Fig. 4. Spectral channel residual images after making the image in Figure 2 **right** which tapered images to comparable resolution. Images cover the same region and and use the same contouring as in Figure 3.

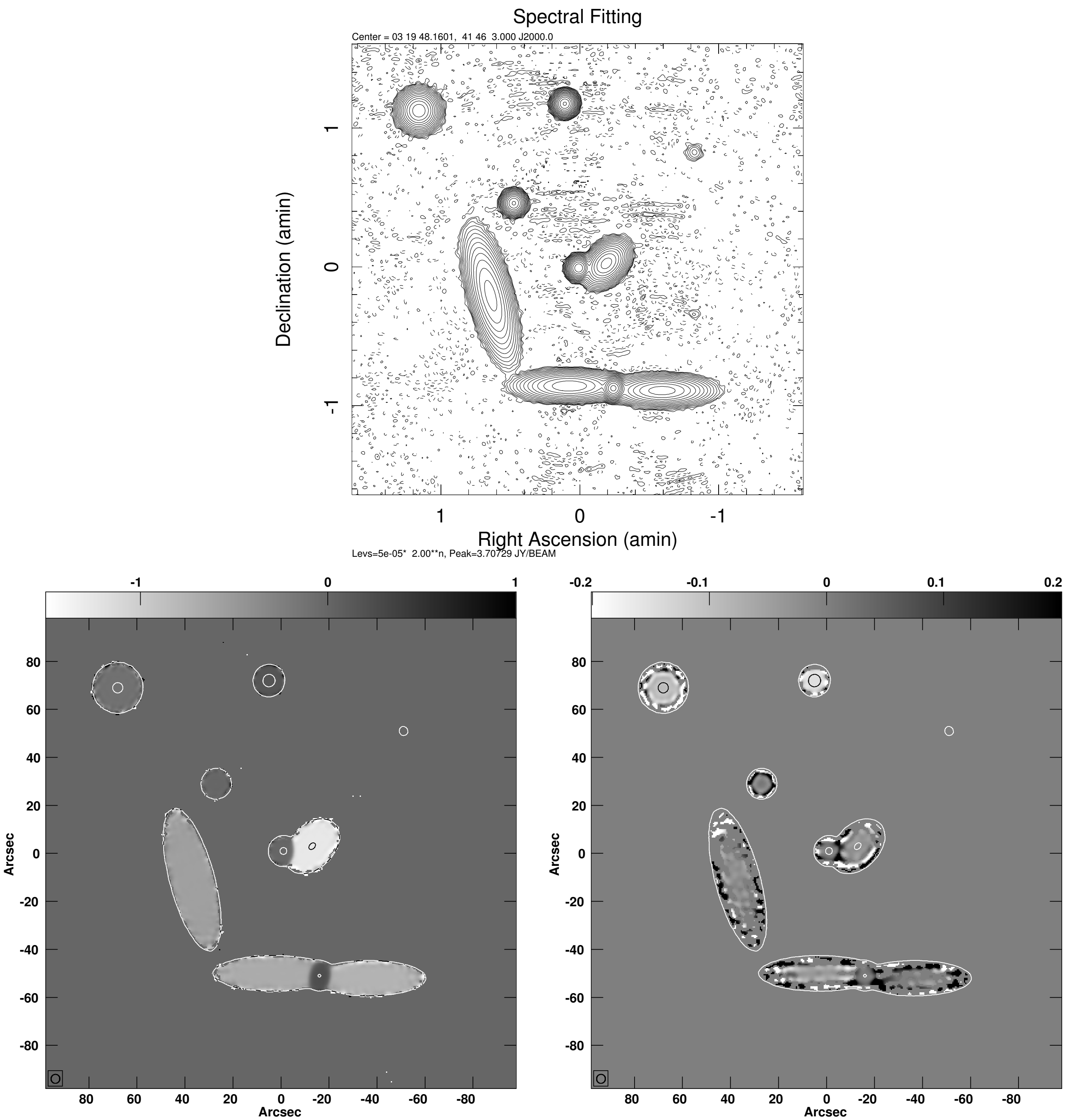

Fig. 5. **Top** Image of test data derived from spectral fitting. Cell spacing is 0.5". The image RMS is 0.031 mJy/bm and dynamic range is 1.2×10^5. Contour levels are powers of 2 from 0.05 mJy/bm, the peak in the image is 3.707 Jy/beam.
Bottom Left: Spectral index for image in Figure 5. Gray-scale is Spectral index with scale bar at top with contours of flux density at 0.5 mJy/bm and 1.0 Jy/bm.
Bottom Right: Same as **Bottom Left** but spectral curvature. This term is less well constrainged than spectral index in regions with low SNR at the edges of components leading to larger fluctuations.

channel images.
  - Restores tabulated spectra on the CLEAN component to channel residuals, cross restoring between facets if needed.
  - Flattens the multiple channel images if multiple facets used.
- **ObitDConCleanPxListMF**
  Derived from ObitDConCleanPxList, this is where the basic component finding is done. Components are selected on the basis of the combined flux density and tabulated spectra are recorded in the CLEAN components written. Both "Clark" and "SDI/Greisen" variants are supported. For Clark CLEAN, the components selected are subtracted from both the combined pixel list and those of the channels.
- **ObitImageMosaicMF**
  Derived from ObitImageMosaic this class contains the images needed to cover the facets and outlying fields. When the mosaic is created or extended, the created images and beams are of type ObitImageMF.
- **ObitImageMF**
  Derived from ObitImage, objects of this class have a frequency–like axis with label SPECLNMF to indicate that the multiple planes are a spectral expansion in $ln(\nu)$ followed by the coarse spectral planes.
  - Function Combine derives the combined image from the channel images; a linear average plus corrections for channel extrema.
  - Function FitSpec does the least squares fitting of the spectra to pixels and writes the appropriate planes in the image.
- **ObitUVImagerMF**
  Derived from ObitUVImager, this class creates ObitImageMFs from UV data. The chief difference is that the multiple channel images are first formed and then the combined image.
- **ObitUVGridMF**
  Derived from ObitUVGrid this grids UV data. The chief difference is that the multiple channel images are formed.
- **ObitSkyModelMF**
  Derived from ObitSkyModel this implements the specialized functions needed to use the CLEAN components with tabulated spectra. Both DFT and Gridded model calculations are implemented.

The user interface is implemented via task MFImage. In addition to the usual Obit imaging task parameters the following are included:

- **maxFBW**
  The maximum allowed IF center fractional bandwidth. This parameter is used to divide the visibility spectrum into image channels. Each IF will have an integral number of channels.
- **doFit**
  If true, the final (CLEAN) spectral planes are fitted and the first order+1 planes are filled with the spectrum
- **norder**
  This specifies the maximum order of imaging to be used; 0=only S_0, 1=$S_0 + \alpha$, 2=$S_0 + \alpha + \beta$
- **Beam**
  The desired target resolution. If not specified, it is determined by imaging the beam of the lowest frequency coarse channel.

Because the result of the CLEAN is a set of CLEAN components with spectral information, all the usual self–calibration facilities are also available. All of the compute intensive operations are multi–threaded leading to a very efficient implementation. The CPU/real ratio on an 8 core computer for the tests reported here were in excess of 6 for the full run of MFImage.

VIII. Discussion

The revisited spectral imaging technique of [5] performs comparably to the earlier tests but the dynamic range in the images produced is too low to warrant further development.

The Spectral Fitting technique as implemented in Obit task MFImage produces a dynamic range, 1.2×10^5, within about a factor of 2 of the best result from [5] on the same dataset but produces a sky model that is usable for self–calibration and similar functions. Among the features of MFImage are:

- Good dynamic range
- Images of spectral index and curvature terms
- Self–cal integrated into imaging
- Corrections for primary beam shape
- Correction for average spectral index
- Automated faceted imaging with 2 or 3D
- Fully threaded implementation
- DFT and Grid models for accuracy or speed
- SDI/Greisen or traditional CLEAN
- Potential for error analysis
- Baseline dependent time averaging
- autoCenter/autoWindow
- Peeling integrated
- Suitable for batch or pipeline processing

As the test images are limited by systematic artifacts rather than noise, further improvement is possible. Further development of wideband self–calibration will also be needed.

IX. Conclusion

A technique is presented that gives good dynamic range ($> 10^5$) results on simulated wide–band interferometric data as well as a sky model usable for self–calibration. Corrections for frequency dependent primary beam gain are included in a natural way. Imaging of a test dataset gave excellent recovery of the input sky model. An efficient, multi–threaded, production capable implementation of this technique is available in Obit.

Acknowledgment

The author would like to thank Ed Fomalont, Huib Intema, Gareth Hunt and Juan Uson for valuable comments, suggestions and discussions on this topic.

References

[1] F. R. Schwab, "Optimal Gridding of Visibility Data in Radio Interferometry," in *Indirect Imaging. Measurement and Processing for Indirect Imaging. Australia, Cambridge University Press, Cambridge, England, New York, NY, L C # QB51.3.E43 I53 1984. ISBN # 0-521-26282-8. P.333, 1983*, 1983, pp. 333–+.

[2] W. D. Cotton, "Special problems in imaging," in *Synthesis Imaging in Radio Astronomy*, ser. ASP Conference Series, R. A. Perley, F. R. Schwab, and A. H. Bridle, Eds., no. 6. Astronomical Society of the Pacific, 1989, pp. 243–246.

[3] R. J. Sault and M. H. Wieringa, "Multi–frequency synthesis techniques in radio interferometric imaging," *Astron. Astrophys. Suppl.*, vol. 108, pp. 585–594, December 1994.

[4] W. D. Cotton and F. R. Schwab, "Attempt to Adapt Sault-Wieringa Deconvolution to High Dynamic Range Imaging," *Obit Developement Memo Series*, vol. 18, pp. 1–11, 2010.

[5] W. D. Cotton, "Towards a Wide–band Spectral Imaging Technique in Obit," *Obit Developement Memo Series*, vol. 3, pp. 1–10, 2008.

[6] ——, "Obit: A Development Environment for Astronomical Algorithms," *PASP*, vol. 120, pp. 439–448, 2008.